

---

# COVID-19 PLATEAU: A PHENOMENON OF EPIDEMIC DEVELOPMENT UNDER ADAPTIVE PREVENTION STRATEGIES

---

A PREPRINT

**Ziqiang Wu**  
 Shenzhen University  
 Shenzhen, China  
 wzqgddg@foxmail.com

**Hao Liao**  
 Shenzhen University  
 Shenzhen, China  
 jamesliao520@gmail.com

**Alexandre Vidmer**  
 Shenzhen University  
 Shenzhen, China  
 alexandre@vidmer.com

**Mingyang Zhou**  
 Shenzhen University  
 Shenzhen, China  
 zhoumy2010@gmail.com

**Wei Chen**  
 Microsoft Research Asia  
 Beijing, China  
 weic@microsoft.com

June 16, 2022

## ABSTRACT

Since the beginning of the COVID-19 spreading, the number of studies on the epidemic models increased dramatically. It is important for policy makers to know how the disease will spread, and what are the effects of the policies and environment on the spreading. In this paper, we propose two extensions to the standard infectious disease models: (a) We consider the prevention measures adopted based on the current severity of the infection, those measures are adaptive and change over time. (b) Multiple cities and regions are considered, with population movements between those cities/regions, while taking into account that each region may have different prevention measures. While the adaptive measures and mobility of the population were often observed during the pandemic, these effects are rarely explicitly modeled and studied in the classical epidemic models. The model we propose gives rise to a *plateau* phenomenon: the number of people infected by the disease stay at the same level during an extended period of time. We show what are conditions needs to be met in order for the spreading to exhibit a plateau period, and we show that this phenomenon is interdependent: when considering multiples cities, the conditions are different from a single city. We verify from the real-world data that plateau phenomenon does exists in many regions of the world in the current COVID-19 development. Finally, we provide theoretical analysis on the plateau phenomenon for the single-city model, and derive a series of results on the emergence and ending of the plateau, and on the height and length of the plateau. Our theoretical results match well with our empirical findings.

**Keywords** COVID-19, Infectious disease model, human mobility, plateau phenomenon

## 1 Introduction

Since December 2019, a virus named SARS-CoV-2 has been affecting the world. As of October 11, 2020, the virus had infected 11,195,010 people, including the UK Prime Minister Boris Johnson and the US President Donald Trump. Although the epidemic in some countries has been brought under control, the epidemic in most part of the world is still ongoing. Nowadays (October, 2020), the number of new cases is still more than 100,000 every day.

The number of studies based on the epidemic analysis has considerably grown since the start of the COVID-19 epidemic. Scholars from different fields usually have been using the infectious disease models to analyze the evolution of the disease and model its future evolution. In a widely used SIR model [1], we distinguish every individual in three different state susceptible (S), infected (I) and recovered (R), hence the name. The susceptible portion of the population

comprises the people who can be infected by the disease, the infected part is the part of the population who is infected and can transmit the disease, while the recovered part is the one who has been out of the spread process.

SIR and related models are well studied in the literature. However, during the COVID-19 pandemic, many regions gradually adopt adaptive prevention strategies to try to balance between epidemic prevention and economic growth, and different regions often employ different prevention strategies. This may bring new phenomenon that does not exist in the standard epidemic models.

In this paper, we propose two extensions to the standard infectious disease models: (a) we consider adaptive changes in prevention strategies based on the current infection severity; and (b) we consider multiple regions with population mobility while each region may employ different prevention strategies. For simplicity, we refer each region as a city henceforth. We first conduct simulation studies on the proposed model using parameters learned from the real-world data, and observe that in many situations the epidemic development has a period where the number of existing infected people stays at the same level, for which we call it a *plateau* period. We discover that in the single-city model, the plateau may only occur under certain conditions, and their heights and length may differ. For example, the height of a plateau seems to be positively correlated with the prevention threshold used to trigger the changes in prevention intensity, but not affected by other prevention measures. In the multi-city model, we discover that the plateau always co-occur among all cities, even when some city's prevention strategy would not generate a plateau in the single city model. We next verify from the real-world data that plateau phenomenon does exists in many regions of the world in the current COVID-19 development, indicating that this is an important phenomenon to study. Finally, we provide theoretical analysis on the plateau phenomenon on the single-city model, and derive a series of results on the emergence and ending of the plateau, and on the height and length of the plateau in the single-city model. Our theoretical results match well with our empirical findings.

To summarize, the key contributions of this paper are as follows:

- we extend the SIR model to incorporate adaptive prevention strategies and population mobility among different regions that also employ different prevention strategies.
- We empirically verify through simulations and real-world data that an important plateau phenomenon exists, and summarize some interesting properties on its appearance and characteristics in the single-city model and relationships among plateaus in the multi-city model.
- We conduct theoretical analysis on the properties of the plateau and our theoretical results match well with the empirical findings.

## 2 Related Works

Most of the existing epidemiological studies based on COVID-19 can be divided into the following four categories.

**Research on the epidemiological characteristics of COVID-19.** Although most of the attributes of SARS-CoV-2 cannot be obtained by epidemic analysis, the epidemiological characteristics of COVID-19 can be estimated. Most of the works [2, 3, 4, 5, 6] focus on the study of the basic reproduction number  $R_0$  of COVID-19, which can reflect the propagation ability of SARS-CoV-2. Other works [7, 8, 9, 10] analyzed the characteristics of COVID-19 such as generation interval (cases doubling time).

**Prediction of the virus trend.** By combining real data with the model, these works aims to predict the development of COVID-19. Since the beginning of the COVID-19 outbreak, it has been a hot topic. The most common method to predict the number of futures infections relies on real-time data [11, 12, 13, 14, 6]. Due to the global characteristics of the epidemic, many focused on combining population mobility data with the spreading model [15, 2, 5, 16, 17].

**Improvement of the epidemic model.** Apart from the population mobility, there are additional aspects that were studied to enhance the quality of the prediction. The SEAIRD model allows for further division of the population [18, 19, 20]. Environmental parameters were also added to the models [21, 22], and machine learning algorithms were used [23, 24].

**Exploration of the effects of prevention measures.** Some countries try their best to prevent COVID-19, while others wait for mass immunity. The significance of prevention has become the subject of many studies [25, 16, 26, 27]. Based on the development of the epidemic situation before and after prevention, the role of prevention was analyzed. Almost all the results affirmed the role of prevention, and pointed out that the epidemic would worsen more seriously without prevention.

These works have studied various aspects of on COVID-19 pandemic, but none of them looked into the effect of adaptive changes of prevention measures over time on the epidemic development, and none of them study the plateau phenomenon that appears in practice. This is the subject of our study that differentiates ours from existing studies.

### 3 Epidemic Model with Prevention Strategy

Traditional epidemic models such as the SIR model [1] do not model behavioral changes in the population that could change the virus propagation dynamics. However, as we have seen with the COVID-19 epidemic, people change their behaviors due to the epidemic either voluntarily or by government restrictions, such as wearing masks, reduce traveling and gathering when the epidemic is getting severe, until the epidemic situation is getting better. Moreover, different geographic regions could impose different prevention strategies, and it is further complicated by the cross-regional population movement.

In this paper, we incorporate the constantly changing prevention measures as well as the population mobility between regions into the SIR model. For the COVID-19 with latent period, we do not choose the SEIR model, because using the SIR model in the process of studying the prevention strategy can simplify the analysis process, and is no different from the SEIR model. For simplicity, we refer regions as cities, but in reality they could represent either cities or provinces, states, counties, or communities.

#### 3.1 SIR-based Single-city Model

Our single-city model is based on the SIR model [1], in which each individual goes through the states of being susceptible (S), infected (I), and recovered or removed (R). The standard SIR model is governed by two parameters — infection rate  $\beta$  and recovery rate  $\gamma$ . To incorporate the prevention strategies and its dynamic changes into the model, we further add a prevention parameter  $r$  into the model. Thus, in our model  $\beta$  is interpreted as the probability that when a susceptible individual interacts with an already infected individual in a time unit, the susceptible individual gets infected from the latter, and  $\gamma$  is the probability that an infected individual recovers from the disease in a time unit, while  $r$  is the number of individuals one infected individual would interact with in one time unit. It is important to remark that in our model,  $\beta$  and  $\gamma$  are the intrinsic properties of the virus, and it is not affected by the prevention measures, while  $r$  is affected by the prevention measures —  $r$  will be smaller if the city imposes higher level of prevention measures and people exercise social distancing, and  $r$  is larger if the city relaxes its prevention measures. The combined  $r\beta$  would correspond to the  $\beta$  parameter in the standard SIR model. Then, the differential equations of the single-city model are as follows:

$$\frac{dS}{dt} = -\frac{r\beta IS}{N}, \quad (1)$$

$$\frac{dI}{dt} = \frac{r\beta IS}{N} - \gamma I, \quad (2)$$

$$\frac{dR}{dt} = \gamma I, \quad (3)$$

where  $S$  is the susceptible population,  $I$  is the infected population,  $R$  is the recovered population,  $N$  is the total population of the city, and  $t$  is the time. Note that  $S, I, R$  are considered variables that change over time, while  $N$  remains the same over time. Equation (1) can be interpreted as the change of  $S$  in a time unit  $dt$  due to the fact that each infected individual meets  $r$  individuals, among them a fraction of  $S/N$  are susceptibles, and thus  $\beta$  fraction of them will be infected and change from  $S$  state to  $I$  state, and since we have  $I$  infected individuals, the total decrease on  $S$  is  $\frac{r\beta IS}{N}$ . Equation (3) is simply because there are currently  $I$  infected individuals and  $\gamma$  fraction of them would be recovered in each time unit  $dt$ , and Equation (2) is the combined effect of the other two equations.

#### 3.2 Multi-city Model

We extend the single-city model to multiple cities where different cities may impose different levels of prevention measures and there are population movement between the cities. In the multi-city model, there are  $m$  cities. For each city  $i$ , we use subscript  $i$  in  $S_i, I_i, R_i, N_i$  and  $r_i$  to represent the SIR variables and parameters. Note that  $\beta$  and  $\gamma$  are the same across cities since they model the intrinsic characteristics of the virus, while the prevention parameter  $r_i$ 's are different across different cities, modeling different prevention measures taken among the cities.

##### 3.2.1 Population balancing with the external environment

In the real world, the population base of a city is usually stable over time. Thus, we would like our model to maintain the population for city  $i$ ,  $N_i$ , the same over time, which also simplifies our model analysis. However, with different population mobility between cities, it is not trivial to maintain population balance in the multi-city model. To achieve this, we introduce the external environment as the background that could counter balance the excess or deficit of population of each city due to the population movement. The external environment could be viewed as other cities that

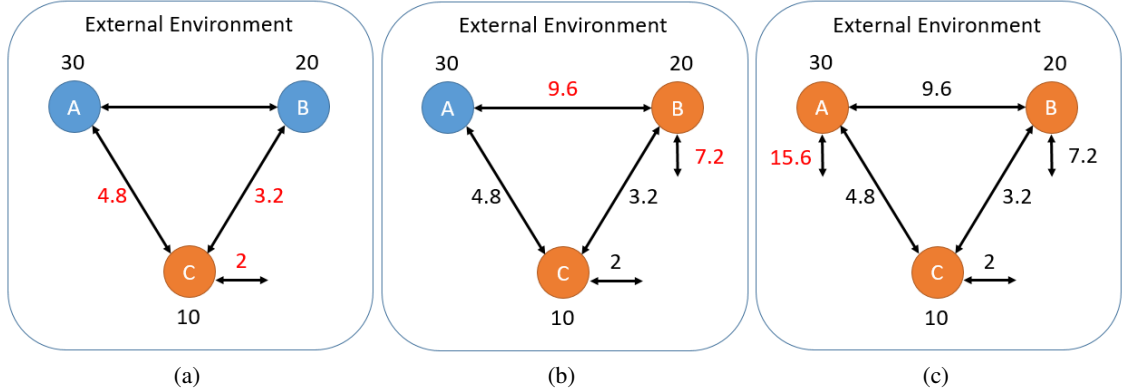


Figure 1: Take city A, city B and city C as examples to demonstrate the rules of population mobility. The number next to the circle is the total floating population of the city, and the number on the side is the floating population between the two cities, in units of thousand people.

we would not model explicitly or the rural areas surrounding the cities. The technical model and mobile population calculation is explained below.

Suppose that each city  $i$  has a *floating population*  $f_i$ , which is a fraction of the total population who will move in or out of the city in a time unit. Let  $f_{i,j}$  be the population moving from city  $i$  and city  $j$  in a time unit, and  $f_{i,0}$  be the population moving between the city  $i$  to the external environment in a time unit. Thus, we have  $f_i = \sum_{j=0, j \neq i}^m f_{i,j}$ . We use the following rules to govern the inter-city population movement: (1) between two cities, the two directional movement population is balanced, i.e.  $f_{i,j} = f_{j,i}$ ; and (2) the population movements from one city  $i$  to two different cities  $j$  and  $j'$  are proportional to the two destination cities' floating populations, i.e.  $f_{i,j}/f_{i,j'} = f_j/f_{j'}$ . To realize the actual values of the population movement, we use the following simple procedure: We first sort the floating population  $f_i$  from the smallest to the largest, and determine the population movement of each city in this order (without loss of generality, assuming  $f_1 \leq f_2 \leq \dots$ ). For the city 1 with the smallest floating population, we first allocate a fixed fraction (e.g. 20%) of the floating population as the exchange population with the external environment to ensure that every city has population exchange with the environment, and the remaining floating population is allocated to  $f_{1,j}$  proportional to the city  $j$ 's floating population  $f_j$ , according to rule (2) above. Then for each remaining city  $i$  in the order, we first apply rule (1) above to fix the  $f_{i,j} = f_{j,i}$  for all  $j < i$ , and then apply rule (2) on the remaining cities  $j' > i$  to get  $f_{i,j'}$  proportional to  $f_{j'}$ , and finally for the left over population  $f_i - \sum_{j=0, j \neq i}^m f_{i,j}$ , we assign it to the exchange population with the environment  $f_{i,0}$ .

Figure 1 shows a concrete example of the procedure. (a) The floating population of city A, city B and city C is 30, 20 and 10 thousand respectively. First of all, the floating population between city C and other cities is calculated, with 20% floating population (i.e. 2,000) exchanges with the environment, and the remaining 80%, or 8,000 is allocated among moving populations to city A and city B. Based on the population proportion, movement to city B accounts for 40%, which is 3,200, and movement to city A is 4,800. (b) Then we calculate the city B with the second smallest floating population. The floating population between city B and city C is 3,200, and the ratio of floating population between city C and city A is 1: 3. Therefore, the proportion of floating population between city B and city C and between city B and city A is also 1:3. The floating population between city B and city A is 9,600, and the remaining 7,200 are between city B and the external environment. (c) Similarly, the remaining 15,600 floating population in city A will be used as the floating population with the external environment.

With the above rules of population mobility, the population base of each city remains unchanged, and the cities with more floating population account for a larger proportion of the floating population in other cities.

### 3.2.2 Multi-city SIR model base on population mobility

We now combine the single-city SIR model with the mobility rules defined in the previous section. With the rules of population mobility and the external environment, we can ensure the dynamic balance of population mobility in multiple cities in the model. By adding the part of floating population to the single-city model, we get the multi-city

model with the following equations:

$$\frac{dS_i}{dt} = -\frac{r_i \beta I_i S_i}{N_i} + \sum_{j=0, j \neq i}^m f_{i,j} \left( \frac{S_j}{N_j} - \frac{S_i}{N_i} \right), \quad (4)$$

$$\frac{dI_i}{dt} = \frac{r_i \beta I_i S_i}{N_i} - \gamma I_i + \sum_{j=0, j \neq i}^m f_{i,j} \left( \frac{I_j}{N_j} - \frac{I_i}{N_i} \right), \quad (5)$$

$$\frac{dR_i}{dt} = \gamma I_i + \sum_{j=0, j \neq i}^m f_{i,j} \left( \frac{R_j}{N_j} - \frac{R_i}{N_i} \right), \quad (6)$$

where  $m$  for the total number of cities, 0 represents the external environment, and  $1 \sim m$  represent the cities. The explanation of the above equations should be straightforward. For example, for Eq. (4), besides the virus infection within the city given by the term  $\frac{r_i \beta I_i S_i}{N_i}$  same as in Eq.(1), we also account for movements between the cities: for every  $j \neq i$ ,  $f_{i,j} S_i / N_i$  is the number of susceptible individuals moving out of city  $i$  to city  $j$ , assuming that the mobile population has the same fraction of susceptible individuals as the general city population; and  $f_{i,j} S_j / N_j$  is the number of susceptible individuals moving into city  $i$  from city  $j$ . The other equations have the similar explanation.

From the model, in particular Eq. (5), we can see that if city  $j$  has a higher portion of infected people than city  $i$ , i.e.,  $I_j / N_j > I_i / N_i$ , then city  $j$  contributes the inflow of infected to city  $i$ , and vice versa. This matches the intuition of virus propagates from highly infected cities to lowly infected cities.

### 3.3 Prevention Strategy

During the epidemic, different cities or regions may have different strategies and measures to deal with infectious diseases. For example, during the COVID-19 outbreak, some regions impose mandatory mask wearings while some do not, many enforce social distancing, but at different scales, such as limited the size of gathering of no more than 50 or 100 people, closing schools, or restricting travels to and from high risk regions. All these restrictions can be reflected into two parameter changes within our model. First is the prevention parameter  $r_i$  for each city  $i$ . Different social distancing measures essentially all reduce the number of people any individual would meet in a time unit, which is modeled by  $r_i$ . Thus we use  $r_i$  to model the prevention measures, with lower  $r_i$  meaning high level of prevention measures and high  $r_i$  meaning low level of prevention measures. Another parameter affected by the prevention measure is the fraction of the floating population  $f_i / N_i$  of each city  $i$ , denoted as  $p_i$  — a higher prevention level decreases the fraction of the floating population while a lower prevention level increases the fraction of the floating population.

Most cities or regions also dynamically adapt their prevention measures based on the current infection data — when the new infection cases rise the prevention measures intensifies, and when the number of new cases drops, the prevention measures is relaxed. We model this scenario by setting an prevention threshold and dynamically change the prevention parameter  $r_i$  and the fraction of the floating population  $p_i$  based on whether the current infection cases is below or above the prevention threshold. Technically, we have three main factors for deciding and changing the prevention measures: (1) *Prevention threshold  $\theta$* , which sets a limit on the number of new infections within a time period. New infections only include new cases caused by intra-city infections, excluding imported cases brought outside the city. When the new number of infected people each day for 14 consecutive days is lower than the prevention threshold, it shows that the epidemic situation is getting under control, and the prevention intensity begin to decline ( $r$  increases). When the number of new infected people in any given day is higher than the prevention threshold, it shows that the epidemic may worsen again, and prevention intensity begin to rise ( $r$  decreases). (2) The *range of changing prevention intensity*  $[r_L, r_H]$  and  $[p_L, p_H]$ , which gives the range of changes of each prevention parameter  $r_i$  and the fraction of floating population parameter  $p_i$ . When the prevention measure intensifies, the values are changed to  $r_L$  and  $p_L$  respectively, and when the prevention measure relaxes, the values are changed to  $r_H$  and  $p_H$ . (3) The speed of the change in prevention intensity, as measured by the number of days  $k$  to complete the change. In the real world, the change of prevention measures never happens instantaneously and it takes some time. So we use  $k$  to model the number of days needed to change  $r_L$  to  $r_H$  and  $p_L$  to  $p_H$ , or in the reverse order. We use the geometric sequence to implement such change sequences, as given below:

$$r_{t+1} = r_t \cdot \left( \frac{r_H}{r_L} \right)^{\frac{(-1)^s}{k}},$$

$$p_{t+1} = p_t \cdot \left( \frac{p_H}{p_L} \right)^{\frac{(-1)^s}{k}},$$

where  $t$  represents days and  $s$  represents the direction of change in prevention. When  $s = 0$ , it means that the prevention intensity is reduced. When  $s = 1$ , it means that prevention intensity is strengthened. The prevention intensity  $r$  and the proportion of floating population  $p$  are always within the range of the prevention strategy.

Table 1: Indicators of prevention strategy.

	$\theta$	$r$ -range	$p$ -range	$k$
PS1	—	$r$	$p$	—
PS2	$\theta$	$[r_L, r_H]$	$[p_L, p_H]$	$k$

\*  $\theta$  indicates the prevention threshold,  $r$ -range indicates the range of changing prevention intensity,  $p$ -range indicates the range of changing proportion of floating population,  $k$  indicates the speed of the change in prevention intensity, and PS indicates prevention strategy.

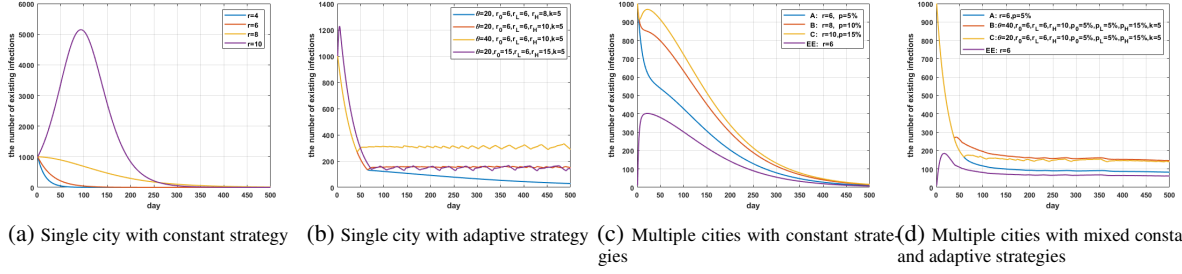


Figure 2: Infectious disease model with constant or adaptive prevention strategies. In the single-city model, the initial condition of the city is  $IC = (200000, 0.5\%)$ , as shown in (a), (b). In the multi-city model, the initial conditions of the three cities A, B and C are all  $IC = (200000, 0.5\%)$ , while the initial condition of the external environment is  $IC = (1000000, 0.01\%)$ . Notations  $r$  and  $p$  represent the constant prevention intensity and the constant proportion of population mobility, respectively. For adaptive strategies,  $r_0$  indicates the initial prevention intensity, while  $r_L$  and  $r_H$  indicate the lower limit and upper limit of the prevention intensity, respectively;  $p_0$  indicates the initial proportion of population mobility, while  $p_L$  and  $p_H$  represent the lower and upper limits of the proportion of population mobility, respectively;  $\theta$  represents the prevention threshold, and  $k$  represents the speed of the change in prevention intensity.

In general, prevention strategies can be summarized like in Table 1. PS1 is the case that the prevention intensity remains unchanged: the parameters of prevention intensity  $r$  and the proportion of floating population  $p$  are fixed values, and there is no prevention threshold and reaction speed. This corresponds to the classical infectious disease model, and we refer to it as a model with a *constant prevention strategy*. PS2 corresponds to the adaptive changes in prevention intensity that we commonly see during the COVID-19 pandemic: the full strategy is characterized by the prevention threshold  $\theta$ , the  $r$ -range  $[r_L, r_H]$ , the  $p$ -range  $[p_L, p_H]$ , and the change speed  $k$ , and we refer to such ones as models with an *adaptive prevention strategy*.

In the next section, we will empirically evaluate our models to discover the key phenomenon of epidemic plateau, and validate it against the real-world COVID-19 data. We will then provide theoretical analysis on the plateau phenomenon in Section 5.

## 4 Empirical Observations — the Plateau Phenomenon

Based on the above epidemic model with prevention strategy, we take the COVID-19 as an example to simulate the epidemic development in a single city and in multiple cities. We will use one day as the time unit for the model given in the previous section.

### 4.1 Experiment Setup

We base the choice of our parameters on the research that have been made on the COVID-19.

#### 4.1.1 Infection rate and recovery rate

The first parameters are the infection rate and the recovery rate of COVID-19. A person stays infected by COVID-19 for 8.4 days on average [2]. The recovery rate is thus defined as  $\gamma = 1/8.4 = 0.12$ . For the infection rate of COVID-19, we use the most common indicator in the epidemic research, the reproduction number to calculate.

The reproduction number can be divided into basic reproduction number and effective reproduction number. The basic reproduction number represents the average number of people infected in a group of all susceptible people before an infected person recovers, expressed as  $R_0$ . The estimation of the basic reproduction number is generally chosen in the early stage of the outbreak, as the proportion of susceptible people in the population is close to 1. The effective reproduction number is different from the basic reproduction number, and it represents the average number of people infected at time  $t$  with a certain proportion of the susceptible population before an infected person recovers, expressed as  $R_t$ . The effective reproductive number  $R_t$  will change over time, because the proportion of susceptible people will change with the development of the epidemic. When the effective reproduction number  $R_t < 1$ , it indicates that the epidemic is receding and will die out soon. The time from infection to the recovery from the infection is an infection cycle, which is  $\frac{1}{\gamma}$  days. Before recovering, the infected person will come into contact with  $r$  individuals every day. Among these people, only susceptible people will be infected, and the probability of each susceptible individual getting infected is  $\beta$ . Therefore, the basic reproductive number  $R_0$  and the effective reproductive number  $R_t$  have the following relationship with infection rate  $\beta$  and recovery rate  $\gamma$ :

$$R_0 = \frac{r\beta}{\gamma}, \quad (7)$$

$$R_t = \frac{r\beta}{\gamma} \cdot \frac{S}{N}. \quad (8)$$

We can get the infection rate  $\beta$  of COVID-19 through the basic reproduction number  $R_0$  of SARS-CoV-2 and the number of human contact  $r$  as in Eq. (7).

Before calculating the infection rate  $\beta$ , it is necessary to know the prevention parameter  $r$ , or the number of human contacts per day. As discussed before  $r$  will change according to the prevention measures. The basic reproduction number  $R_0$  should corresponds to the situation of the early stage of the outbreak before prevention. At this time, the proportion of susceptible people is close to 1, and the number of contacts with the population is at the normal level. In order to better estimate the number of human contacts, we used the epidemic data provided by the Information Center of Shenzhen Public Security Bureau. In Shenzhen, for people infected with COVID-19, the Public Security Bureau will track down the people who have been in contact with him during the incubation period and conduct medical observation to avoid further spreading. The Public Security Bureau records the number of contacts tracked every day and refers to the number of people obtained as the number of medical observers. Based on the number of daily medical observations, divided by the product of the number of new diagnoses per day and the incubation period (3.0 days), we estimate the normal number of contacts among people  $r = 24$ . In order to make the results closer to the normal number of human contact, the data from the early stage of the epidemic (the first 5 days of the outbreak in Shenzhen) were selected in the experiment.

There are some estimates of the basic reproduction number  $R_0$  in the articles about COVID-19, and the results are all around 3 [2, 3, 4, 5, 14]. Assuming that the basic reproduction number of SARS-CoV-2  $R_0 = 3$ , combined with the recovery rate  $\gamma = 0.12$  and the contact times of the population  $r = 24$ , the infection rate of COVID-19 can be obtained as  $\beta = 0.015$  from Eq. (7).

#### 4.1.2 The number of population contacts and the proportion of population mobility

As derived above,  $r = 24$  is the number of contacts without prevention. The prevention strategies would reduce  $r$ . Only when the effective reproduction number  $R_t < 1$ , the epidemic begins to subside, and the number of infections declines. We call the number  $r$  that corresponds to  $R_t = 1$  as  $\tilde{r}_t$ , the effective prevention intensity, which corresponds to the effective reproduction number  $R_t$  according to Eq. (8). Based on Eq. (8) and the calculated infection rate and recovery rate from above, we can obtain that the number of infections will decrease immediately when the prevention intensity  $r < 8$ .

With the assistance of the Information Center of Shenzhen Public Security Bureau, the population mobility ratio  $p$  is estimated according to the population mobility data of Shenzhen in 2019 and 2020. During the outbreak of COVID-19 in 2020, Shenzhen implemented strict restrictions on population mobility, and the proportion of population mobility was around 5%. In the same period in 2019, the proportion of people moving fluctuated between 10% and 20%. In this paper, it is assumed that the proportion of population mobility under normal conditions is  $p = 20\%$ .

#### 4.1.3 Initial condition.

In the simulation experiment, the total population and the proportion of initial infected people in the city are called initial conditions. Different initial conditions will appear in the single-city model and the multi-city model. An initial condition can be expressed as  $IC = (N, \frac{I_0}{N})$ .

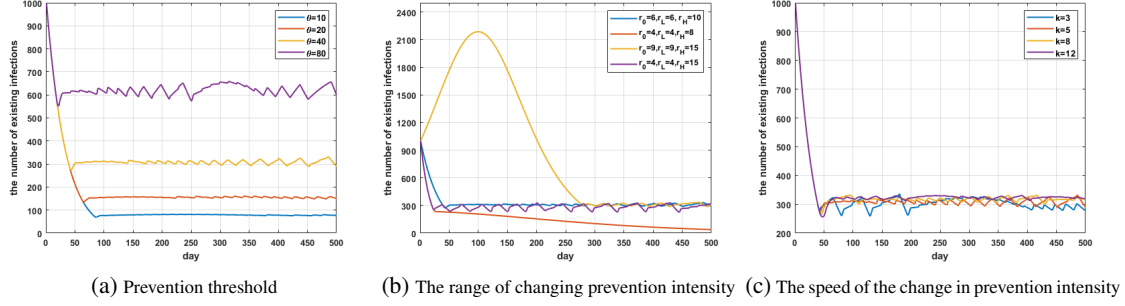


Figure 3: The influence of various indicators on the plateau. In the single-city model, the initial condition of the city is  $IC = (200000, 0.5\%)$ . (a) Prevention threshold  $\theta$  is the indicator for comparison, other indicators  $r_0 = 6, r_L = 6, r_H = 10, k = 5$ . (b) The range of changing prevention intensity  $[r_L, r_H]$  is the indicator for comparison, other indicators  $\theta = 40, k = 5$ . (c) The speed of the change in prevention intensity  $k$  is the indicator for comparison, other indicators  $\theta = 40, r_0 = 6, r_L = 6, r_H = 10$ .

## 4.2 Simulation Results

Figure 2 shows the development of the epidemic in single city and multiple cities with constant or adaptive prevention strategies. The y-axis is the value of  $I$  for a particular day, which is the number of current existing infected individuals that can still transmit the disease (note that it is not the number of newly infected cases in that day). As a convention, for a constant prevention strategy that does not change  $r$ , e.g.  $r$  is always 6, we denote it as  $r = 6$  in the figure legend; for an adaptive prevention strategy, if we initially set a prevention strategy to be at a certain level e.g. 6, and then it will change in the range  $[r_L, r_H]$  when the newly infected case per day drops below the threshold, we denote it as  $r_0 = 6$  and  $r_L, r_H$  to the appropriate values in the legend. The fraction of floating parameter  $p$  and the corresponding  $p_0$  and  $p_L, p_H$  are treated in the same manner.

The results from Figure 2 are as follows.

- Figure 2(a): In the single-city model with a constant prevention strategy, the change curve of the number of existing infections is smooth. The number of infections either continues to decline ( $r \leq 8$ ), or rises first and then falls ( $r > 8$ ).
- Figure 2(b): In the single-city model with an adaptive prevention strategy, the change curve of the number of existing infections is no longer smooth. Comparing to the single-city model with a constant prevention strategy (Figure 2(a)), it has a distinctive feature — a long period in which the number of existing infected people remains more or less the same, with small fluctuations. We refer to such a flat period a plateau, and it is the main phenomenon we are going to study in this paper.
- Figure 2(c): This is the three city case and all cities have constant prevention strategies. In the multi-city model, it can be found that the urban epidemic situation affects each other under the influence of population mobility. The number of infections in city C should have risen to a higher level ( $I > 5000$ ), but instead it begins to decline earlier under the influence of other cities. On the contrary, there has been an increase in the number of infections in the external environment EE which should have been declining ( $r = 6$ ). There is no plateau phenomenon in this case.
- Figure 2(d): In this case, two of the cities (B and C) adopt adaptive prevention strategies, and one city (A) as well as the external environment use a constant prevention strategy. The phenomenon of horizontal fluctuation in the number of existing infections, i.e. the plateau, appears again. More interestingly, the plateau appears in every city, has occurred in every city and the environment, even if some city and the environment adopt a constant prevention strategy.

### 4.2.1 Plateau

As shown in Figure 2, in some cases we see that the phenomenon of plateau may occur, that is, there is a prolonged period in which the number of existing infections maintains at the same level with small fluctuations. The plateau means that there will be a prolonged period in which the infection within the population will be maintained at the steady level. We will see in the next subsection that indeed we could observe such plateau phenomenon in the real-world COVID-19 epidemic. The emergence and the properties of such plateaus are certainly important for the public health authorities to devise appropriate policies to battle against the COVID-19 pandemic. In this section, we will use empirical observations

to extract the possible conditions for the emergence of the plateau and its properties, and in Section 5, we will provide theoretical analysis to validate these observations.

First, from Figure 2, we can see that the adoption of adaptive prevention strategies is strongly correlated to the emergence of the plateau. When there is no adaptive prevention strategies deployed, we do not see the plateau phenomenon. However, the adoption of adaptive strategies itself is not sufficient to guarantee the appearance of the plateau, which can be seen in the blue curve in Figure 2(b). Moreover, in the multi-city situation, even if some city does not adopt an adaptive prevention strategy, it still exhibits a plateau (city A in Figure 2(d)), seemingly under the influence from other cities with adaptive prevention strategies. Thus, the actual condition of the emergence of plateau needs to be further analyzed.

Second, the height of the plateau is different with different adaptive prevention strategies. In the next test, we will try different prevention strategies parameters to empirically verify the factors that affect the height of the plateau.

#### 4.2.2 The effect of prevention strategies

From Figure 2, we can see that the adaptive prevention strategies affect the appearance of the plateau. Now we also try different prevention parameters to see their effect on the plateau, especially on the height of the plateau. We use single-city model for this test to make the effect of prevention strategies more direct. As stated in Section 3.3, in the single-city model, an adaptive prevention strategy consists of parameters of prevention threshold  $\theta$ , range of prevention intensity  $[r_L, r_H]$  and the speed of change  $k$  in the number of days to switch the prevention intensity. We now analyze the effect of each of these parameters.

**Prevention threshold  $\theta$ .** As shown in Figure 3a, when there is a plateau in the development of the epidemic, it can be found that the prevention threshold  $\theta$  is positively correlated with the height of the plateau. The greater the prevention threshold, the higher the plateau. A closer look at their relationship, one may even see a close to linear relationship between the prevention threshold and the height of the plateau. We will validate this relationship in the theoretical analysis section. In addition, the higher the plateau, the greater the daily fluctuation of the number of existing infections, but in general it still remains at a certain level.

**The range of changing prevention intensity  $[r_L, r_H]$ .** As shown in Figure 3b, when there is a plateau in the development of the epidemic, different  $[r_L, r_H]$  will not change the height of the plateau. However,  $[r_L, r_H]$  will determine whether the plateau occurs. When both  $r_L$  and  $r_H$  are small, the plateau does not occur, and the number of existing infections continues is declining (see the red line). When both  $r_L$  and  $r_H$  are large, the number of existing infections will rise at first and then decrease, but there will still be a plateau in the end (see the yellow line). The size of the changing range does not affect the height of the plateau, but it is related to the amplitude. The greater the range of change, the greater the amplitude (compare the blue line with the purple line).

**The speed of the change in prevention intensity  $k$ .** Figure 3c shows that  $k$  does not affect the height of the plateau, but it does affect the fluctuation amplitude of the plateau. The smaller the  $k$ , the greater the fluctuation of the number of existing infections during the plateau (compare the blue line with the purple line).

Through our simulations, we can see that the emergence of plateau is related to the range of changing prevention intensity  $[r_L, r_H]$ , and the height of plateau is positively correlated with prevention threshold  $\theta$ . It shows that the integration of prevention strategies, especially the adaptive ones, would change the dynamics of the epidemic that is not covered by the traditional epidemic models. The plateau and its related phenomenon is actually more consistent with what happens in the real world for the COVID-19 pandemic, as we illustrate in Section 4.3.

#### 4.2.3 Results and Discussion on the Multi-city Model

As shown in Figure 2d, it is found that the platform period also exists in the multi-city model. Through simulation and empirical observation, we found the following phenomena.

- The height of plateaus change from the single-city model: In the multi-city model, if all cities have the same  $IC$  and adopt adaptive prevention strategies, they all have a plateau, but the height of the plateau is different from that of the single-city model. Comparing Figure 4(a) with Figure 3a, the height of the plateau of city A decreased, while that of city C increased. The reason is due to the population mobility in the multi-city model. As the proportion of infected people in city A is the highest, the outflow of infected people is larger than the inflow, and the number of infected people in city A will decrease, i.e. the height of the plateau of city A will decrease. City C is the opposite.
- Cities that would not have a plateau by itself could have a plateau in the multi-city model: Cities with constant prevention strategies could also enter a plateau period in the multi-city model. In Figure 4(b), both city A and

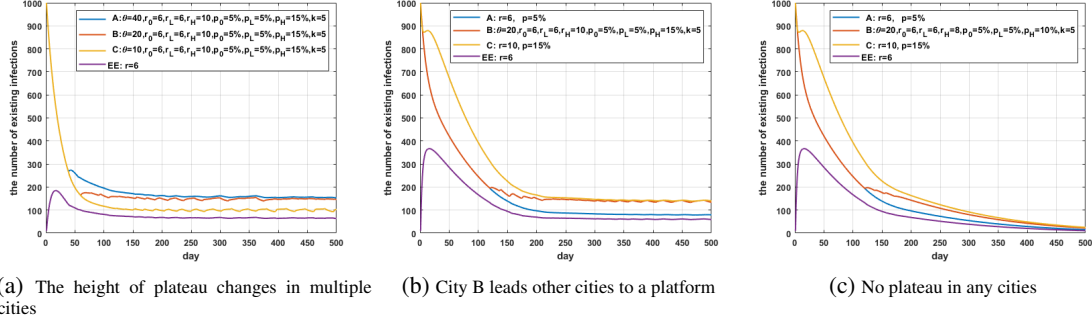


Figure 4: The phenomena of the plateau in multi-city model. Initial conditions of city A, city B and city C are all  $IC = (200000, 0.5\%)$ , while the initial condition of the external environment EE is  $IC = (100000, 0.01\%)$ .

city C adopt constant prevention strategy, in which the number of infections in city A should rise at first and then decline, and the number of infections in city C should be declining all the time, as shown in Figure 2a. However, under the influence of population mobility and city B, every city has entered a plateau. We infer that in the multi-city model, one city have plateau, then it is possible to lead other cities to enter the plateau period.

- Either all cities are in the plateau or none of them is in the plateau: In the multi-city model, Comparing Figure 4(c) with Figure 4a & 4b, we find that the epidemic development in cities is not independent. Either every city has entered a plateau (See Figure 4a & 4b), or every city keeps receding without a plateau after their initial peaks.

The above observations show that quite interesting plateau phenomenon emerges even in the multi-city model with complex epidemic dynamics within cities and population mobility dynamics cross cities. In particular, the results strongly indicate that all cities are interdependent in terms of the epidemic development — their plateau phenomenon co-occur, and even a city that would not have a plateau by itself would enter a plateau under the influence from the adaptive strategies of other cities. This suggests that in battling the COVID-19 pandemic, one should not look only at the local prevention strategies, but also need to take into account other regions's strategies and population mobility, and perhaps some global coordination would be more effective.

#### 4.3 Real World Data Verification

The plateau phenomenon also appears in the real world epidemic, in particular in the current COVID-19 pandemic. We collect the epidemic data from the total of 189 countries from data source DXY<sup>1</sup>, which collects data from sources including the World Health Organization (WHO), with data up to the date of October 11, 2020. We visually investigated the data and found that there are 35 countries that have demonstrated clear plateau phenomenon for more than one month. Among other countries, 129 of them are still suffering worsening situations or are facing a new rising of the epidemics, and 10 countries have receding epidemic. The basic statistics are summarized in the following table.

Table 2: Epidemic situation in various countries.

	plateau	worsening	receding
countries	35	129	10

Figure 5 shows a few examples of countries that have a clear plateau phenomenon, including Thailand, South Korea, Tajikstan and Qatar. These data clearly support the existence of the plateau phenomenon in practice, which means it is important for us to study in more details on the plateau phenomemon. Although it may be difficult to pin point the exact reasons that cause the plateau phenomenon for each country, from our simulation result observations, we believe that the plateau phenomenon in these countries is likely related to the adaptive prevention strategies adopted by the countries.

For the majority of countries that are still experiencing worsening COVID-19 epidemic, if proper adaptive prevention strategies are enforced, we could expect that they will also enter the plateau period in the future. Thus, understanding

<sup>1</sup><https://github.com/BlankerL/DXY-COVID-19-Data>

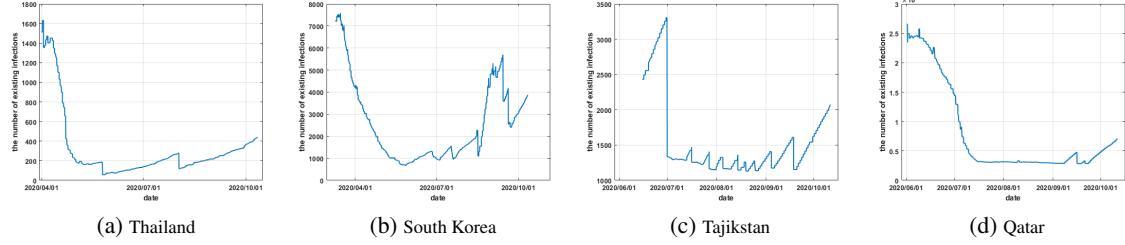


Figure 5: Examples of countries that have a clear plateau phenomenon. The number of existing infections is calculated by the confirmed cases, minus the sum of recovery cases and death cases.

the plateau phenomenon would be useful for most countries that are suffering the COVID-19 epidemic. In the next section, we will provide theoretical analysis on the plateau phenomenon.

## 5 Theoretical Analysis

In the simulation study, we found that epidemic development might enter a plateau period after SIR model is integrated with an adaptive prevention strategy. The simulation study suggests some simple relationships such as the emergence of plateau is related to the changing range of prevention intensity  $[r_L, r_H]$ , and the height of plateau is positively correlated with the prevention threshold  $\theta$ . In this section, we will analyze theoretically the conditions of the emergence and ending of the plateau as well as the properties of the plateau. Our analysis focus on the single-city model. The multi-city model involves much more complicated dynamics due to the mobile populations between the cities and we will leave its theoretical analysis as a future work item.

### 5.1 Effective Prevention Strategy and the Ideal Model

As suggested from the simulation study, the plateau is related to the adaptive prevention strategy, but it is also the case that not every prevention strategy would generate a plateau (See Figure 3b). A closer investigation shows that this is related to the effective prevention intensity  $\tilde{r}_t$ , as defined in Section 4.1.2. Recall that the effective prevention intensity  $\tilde{r}_t$  is the value of prevention intensity  $r$  when the effective reproduction number  $R_t$  takes the value of 1. Intuitively, when  $R_t = 1$ , the number of infections an infected individual makes before he/she is recovered is exactly 1, meaning that the number of existing infected cases would remain the same. Thus,  $\tilde{r}_t$  is the corresponding prevention intensity level that would maintain the infection cases the same. Note that in general the effective prevention intensity  $\tilde{r}_t$  is different from the actual value of the prevention intensity  $r$  used: the former is the would-be value to keep the infection cases the same while the latter is the actual value of the prevention strategy used at each day, and this is also the reason we use different notations to distinguish the two. The effective prevention intensity  $\tilde{r}_t$  has the following simple but important property:

**Lemma 1** *The effective prevention intensity  $\tilde{r}_t$  is monotonically increasing with time  $t$ .*

**Proof 1** *By Eq. (8), and the fact  $\tilde{r}_t$  is defined as the value of  $r$  when  $R_t = 1$ , we have*

$$\tilde{r}_t = \frac{N \cdot \gamma}{S \cdot \beta}. \quad (9)$$

*Since the number of susceptible people  $S$  is monotonically decreasing with time  $t$  while other parameters  $N, \beta, \gamma$  stay constant, we have that  $\tilde{r}_t$  is monotonically increasing.*

In the single-city model summarized in Section 3, we have several aspects that try to reflect the real-world scenario, such as the 14 day grace period before relaxing the prevention intensity, and the changing of the strategies taking some time governed by parameter  $k$ . To emphasize the essence of the model, for the theoretical analysis, we consider the following simplified *ideal* single-city model, which is consistent with the principle of full model. In the ideal model, once the daily new cases drop to the prevention threshold  $\theta$ , we immediately adjust the prevention strategy  $r$  such that we keep the daily new cases to be exactly  $\theta$ , as long as we have  $r \leq r_H$ . Moreover, we assume that the city starts with a significant number of infected cases and under intense prevention control, and thus the prevention strategy is relaxed when the infection cases drop below the prevention threshold. Technically we require that the initial infection number  $I_0$  satisfies  $I_0 \cdot \gamma > \theta$ , that is, the number of daily infected people initially is  $I_0 \cdot \gamma$  and it is more than  $\theta$ . This

corresponds to the real-world scenario where the prevention strategies are only employed after the epidemic outbreak already begins, and the adaptive strategies are designed to maintain the infection cases at a low level after the initial infection peak already occurs. Note that the above description on the ideal model only applies to the adaptive prevention strategy. The constant prevention strategy remains the same in the ideal model. We will also use the simulation results from the full model to validate the accuracy of the prediction from the ideal model.

## 5.2 The Emergence and Ending of Plateau

We first investigate the conditions for the presence or the absence of the plateau, in the single-city model. Let  $t_\theta$  be the time when the number of daily recovered people drops to  $\theta$ , i.e.  $I\gamma = \theta$ . Recall that we assume that initially  $I_0\gamma > \theta$ , and thus  $I$  will eventually drop to  $\theta$ . With Lemma 1, we can derive the following result connecting the effective prevention intensity with the plateau phenomenon.

**Theorem 1** *In the ideal single-city model with an adaptive prevention strategy, at any time  $t$ , if the effective prevention intensity at this time  $\tilde{r}_t \geq r_H$ , then there will be no plateau after time  $t$ . On the other hand, if  $\tilde{r}_{t_\theta} < r_H$ , then there will be a plateau starting at  $t_\theta$ .*

**Proof 2 (Proof (Sketch))** *When  $\tilde{r}_t \geq r_H$ , we know that for any time  $t' > t$ ,  $\tilde{r}_{t'} > \tilde{r}_t$  according to Lemma 1. This means that for all time  $t' > t$ , the actual prevention intensity  $r$  as the property that  $r \leq r_H < \tilde{r}_{t'}$ . Since  $\tilde{r}_{t'}$  corresponds to the effective reproduction number  $R_{t'} = 1$ , this implies that  $R_{t'} < 1$  by Eq. (8), which in turn implies that for all time  $t' > t$ , the number of new infections any infected people would generate is less than 1, and the epidemic will keep receding.*

*Now suppose that  $\tilde{r}_{t_\theta} < r_H$ . According to the definition of  $\tilde{r}_{t_\theta}$ , at time  $t_\theta$   $I\gamma = \theta$ . Let  $t_0$  be the time when the daily infected people first hits  $\theta$ . By our assumption, at time  $t_0$  the infected people  $I$  is dropping from  $I_0$  with  $I_0\gamma > \theta$ . Thus at time  $t_0$   $I\gamma > \theta$  since in the days before  $\theta$ , the daily infected people must be greater than  $\theta$ . This means  $t_0 < t_\theta$ . This implies that before time  $t_\theta$  the ideal model would already adjust  $r$  to keep the daily infection number as  $\theta$ . The condition  $\tilde{r}_{t_\theta} < r_H$  guarantees that it can keep the daily infection number as  $\theta$  to time  $t_\theta$ , at which the daily infection number balances with the daily recovery number  $I\gamma$ . From time  $t_\theta$  on, we can always keep the prevention intensity  $r$  as  $\tilde{r}_t$  until it increases to  $r_H$ . During this period, the daily infection and daily recover balance each other, and we have the plateau.*

The above theorem shows that the relationship of the effective prevention intensity  $\tilde{r}_t$  and the upper bound of the prevention intensity range  $r_H$  directly determine the presence of the plateau. Note that for a constant prevention strategy with a fixed value  $r$ , it is clear that it has no plateau because it is essentially the same as the standard SIR model. Therefore, we can obtain the following conclusion on the emergence and the ending of the plateau.

**Corollary 1 (Condition for the emergence of the plateau)** *In the ideal single-city model, the condition that the plateau will emerge is that we use an adaptive prevention strategy and  $\tilde{r}_{t_\theta} < r_H$ .*

**Corollary 2 (Condition for the ending of the plateau)** *In the ideal single-city model, given that there is a plateau at time  $t$ , the plateau period will end at time  $t' > t$  when  $\tilde{r}_{t'} \geq r_H$ .*

Corollary 1 states that we will have a plateau when the effective prevention intensity is still less than  $r_H$  when the daily recovery number hit the prevention threshold, while Corollary 2 states that when it happens, the plateau will end once the effective prevent intensity reaches  $r_H$ . We defer the discussion on the actual calculation of the condition  $\tilde{r}_{t_\theta} < r_H$  to Section 5.4 when we study the length of the plateau.

We use simulation results shown in Figure 6 to validate these conditions in our actual model. Figure 6a shows the epidemic development under two adaptive prevention strategies. The first strategy, shown in the blue curve, has a clear plateau period. In Figure 6b, we show the corresponding changes of the effective prevention intensity and the actual prevention intensity. For the blue curve in Figure 6a, the blue curve in Figure 6b shows the corresponding changes in the actual prevention intensity  $r$ , which fluctuates between  $r_L = 6$  and  $r_H = 10$  for a period of time. During this period, the yellow curve, corresponding to the effective prevention intensity  $\tilde{r}_{t,1}$  of the first strategy increases gradually from 8 to 10. Since  $\theta = 40$  and  $\gamma = 0.12$ , when y-axis  $I$  is about  $40/0.12 \approx 333$ , the corresponding the effective prevention intensity is around 8, which is less than  $r_H = 10$ , which is consistent with Corollary 1 that the plateau would appear. When  $\tilde{r}_{t,1}$  increases to  $10 = r_H$ , we can see that the plateau ends in the corresponding blue curve on the left. Now, for the second strategy, the red curve in Figure 6a, we see that there is no plateau. The actual prevention intensity  $r$  keeps at the level  $r_H = 8$  in this case (the red curve in Figure 6b), while the effective prevention intensity  $\tilde{r}_{t,2}$  starts at 8 and increases slowly above 8 (the purple curve in Figure 6b). This is also consistent with Corollary 1, meaning that when  $\tilde{r}_{t_\theta} \geq r_H = 8$ , there will be no plateau in this case.

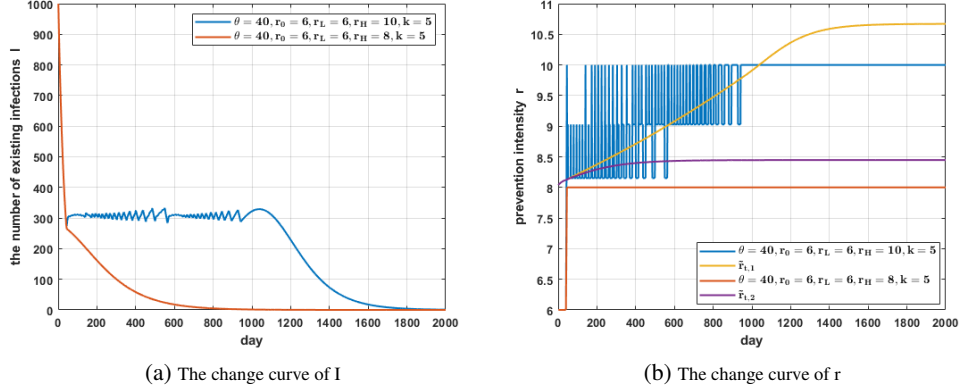


Figure 6: The relationship between the emergence and ending of the plateau and the change of prevention intensity. In the single-city model  $IC = (200000, 0.5\%)$ , the experimental results of different range of changing prevention intensity  $[r_L, r_H]$  show that one has a plateau and the other does not.  $\tilde{r}_{t,1}$  expressed the changes in the effective prevention intensity of the first prevention strategy during the development of the epidemic.  $\tilde{r}_{t,2}$  stands for the second prevention strategy.

### 5.3 The Height of the Plateau

Although the number of infected people in the plateau period has small fluctuations, it is basically maintained at a same value. We call the value around which the number of existing infections fluctuates is the height of the plateau, and denote it as  $I_P$ . In the ideal model, the height of the plateau  $I_P$  is when the number of existing infected people does not change, that is, when the effective reproduction number  $R_t = 1$ . Using the relations we derived before, we can obtain the following result on  $I_P$ .

**Theorem 2** *In the ideal single-city model, the height of the plateau is given as follows:*

$$I_P = \frac{\theta}{\gamma}, \quad (10)$$

where  $\theta$  is the prevention threshold and  $\gamma$  is the recovery rate.

**Proof 3** *In the ideal model, in the plateau we have  $R_t = 1$ , and the daily newly infected people is exactly equal to the prevention threshold  $\theta$ . According to the SIR model the daily newly infected people is  $\frac{r\beta IS}{N}$  (excluding the number of recovered people), and thus in the plateau period,*

$$\theta = \frac{r\beta I_P S}{N}. \quad (11)$$

From Eq. (8), and setting  $R_t = 1$ , we know that  $\frac{r\beta S}{N} = \gamma$ . Plugging it into Eq.(11), we have  $I_P = \theta/\gamma$ .

Theorem 2 directly shows that the height of the plateau has positive linear relationship with the prevention threshold  $\theta$ , and it is not related to the other parameters such as the range of prevention strategy  $[r_L, r_H]$  or the speed of prevention  $k$ . This result is consistent with our simulation study findings (see Figure 3). In particular, comparing with Figure 3a, when we plug in  $\theta = 10, 20, 40, 80$  with  $\gamma = 0.12$ , we obtain the theoretical heights as  $I_P = 83, 167, 333, 667$ , while the empirical averages we obtain the simulation results are 77, 154, 308, 622 respectively, indicating that the theoretical results match with the simulation results reasonably well. The reason that the empirical results are consistently lower than the theoretical predictions is because in our actual model, we have an asymmetric strategy adjustment: we need 14 consecutive days of new cases dropping below  $\theta$  to relax the prevention, while we only need one day of new cases rising above  $\theta$  to strengthen the prevention. This asymmetric control push the actual height lower than our theoretical prediction from the ideal model.

### 5.4 The Length of the Plateau

After obtaining the height of the plateau  $I_P$ , we can further calculate the length of the plateau by the Area Method. We denote the length of the plateau, i.e. the time period from when the plateau begins to the plateau ends, as  $T$ . It is clear that  $T \cdot I_P$  is the area covered under the plateau period. So, we just need to calculate the area underlying the plateau to get  $T$ . The result is given in the following theorem.

Table 3: The empirical and theoretical lengths of the plateau for settings in Figure 3a.

$\theta$	10	20	40	80
days (empirical)	3,929	1,975	1,002	514
days (theoretical)	3,637	1,830	927	475

**Theorem 3** *In the ideal single-city model, assuming that the number of new infections falls to  $\theta$  is the beginning of the plateau period, the length of the plateau is given as follows:*

$$T = \frac{S_B - S_E}{\theta}, \quad (12)$$

where  $S_E$  is the number of susceptible people when the plateau ends, and  $S_E = \frac{\gamma N}{\beta r_H}$ , and  $S_B$  is the number of susceptible people when the plateau begins, and it is the solution of the following equality

$$S = (S_0 + I_0) - I_P + \frac{N\gamma}{r_0\beta} \ln \frac{S}{S_0}, \quad (13)$$

where  $S_0, I_0$  are the number of susceptible and infected people when the time starts, and  $r_0$  is the initial prevention intensity used before the prevention intensity is adjusted in the range  $[r_L, r_H]$ .

**Proof 4 (Proof (Sketch))** *In the curve with  $I$  as y-axis and time as x-axis, the area under curve (AUC) by time  $t$  is the cumulative existing infected people by time  $t$ . On average, each infected individual takes  $1/\gamma$  time to recover, so each infected individual is counted  $1/\gamma$  times. Therefore, the AUC by time  $t$  is the total number of once infected people multiplied by  $1/\gamma$ , which is  $(I + R)/\gamma$ . Since  $S + I + R = N$ , so we have the AUC by time  $t$  is  $(N - S)/\gamma$ . Let  $t_B, t_E$  be the time when the plateau begins and ends, and correspondingly  $S_B$  and  $S_E$  are the numbers of susceptible people at time  $t_B$  and  $t_E$  respectively. Then we have the AUC between  $t_B$  and  $t_E$  is  $(N - S_E)/\gamma - (N - S_B)/\gamma = (S_B - S_E)/\gamma$ . Since the height of the plateau is  $\theta/\gamma$  by Theorem 2, we know the length of the plateau  $T = \frac{(S_B - S_E)/\gamma}{\theta/\gamma} = \frac{S_B - S_E}{\theta}$ . Thus Eq.(12) holds.*

We now show how to derive  $S_B$  and  $S_E$ . First, for  $S_E$ , we know from Corollary 2 that when the plateau ends,  $\tilde{r}_{t_E} = r_H$ , and by the definition of  $\tilde{r}_{t_E}$ , we know  $R_{t_E} = 1$ . Plugging these values into Eq. (8), we obtain that  $S_E = \frac{\gamma N}{\beta r_H}$ .

To derive the result for  $S_B$ , we rely on the equation below connecting  $I$  and  $S$  in the SIR model [28]:

$$I = (S_0 + I_0) - S + \frac{N\gamma}{r\beta} \ln \frac{S}{S_0},$$

where  $S_0, I_0$  are the numbers of susceptible and infected people when the time starts. Before entering the plateau period, the prevention intensity  $r$  is fixed to a value  $r_0$ . When it first hits the plateau period,  $I$  is equal to  $I_P$ . Thus, when plugging  $I = I_P$  and  $r = r_0$  into the above equation, we obtain Eq.(13), and  $S_B$  is the solution of this equation.

Note that  $S_B$  derived from Eq. (13) can be used to test condition  $\tilde{r}_{t_\theta} < r_H$  in Corollary 1:  $\tilde{r}_{t_\theta} = \frac{N \cdot \gamma}{S_B \cdot \beta}$  according to Eq.(9).

We now validate Theorem 3 with the empirical results. We compare our theoretical prediction on the plateau length with the empirical results from Figure 3a, with the initial condition  $IC = (200000, 0.5\%)$  and parameters  $r_0 = 6, r_L = 6, r_H = 10, k = 5$  and  $\theta$  from 10 to 80. Table 3 summarizes the comparison result. We can see that the theoretical and empirical results match reasonably well. Moreover, the estimation error is mainly from the error in the estimation of the height — if we replace the theoretical heights with the empirical heights, we get much closer estimates of 3920, 1984, 1002, 509 respectively, which means our theoretical AUC prediction is quite accurate.

## 6 Conclusion and Future Work

In this paper we study a phenomenon of epidemic development: COVID-19 plateau. This phenomenon is formed under the change of prevention intensity of adaptive prevention strategies. In the traditional infectious disease model, it is difficult to find the existence of the plateau. We investigate empirically from both simulations and real-world data and on the plateau phenomenon, in both single-city models and multi-city models, and further provide theoretical analysis in the single-city model and obtain an number of results on the emergence and the characteristics of the plateau phenomenon. Our results also suggest that all regions are interconnected and local prevention strategies would have

effects to other regions as well. Understanding the plateau phenomenon would be useful for most countries that are suffering the COVID-19 epidemic.

There could be some future work along this direction. On the empirical side, one could investigate in more detail the real-world plateau phenomenon and their correlations with specific prevention strategies used. On the theoretical side, the multi-city model is much more challenging due to the complicated population mobility dynamics, and it would be very important and beneficial to obtain some insightful results in the multi-city model. We hope that our findings could help the understanding of the COVID-19 pandemic (and other epidemics as well) in connection with different prevention strategies, and assist policy makers in predicting the effect of their prevention strategies.

## References

- [1] M. E. J. Newman. *Networks*. Oxford University Press, 2010.
- [2] Joseph T Wu, Kathy Leung, and Gabriel M Leung. Nowcasting and forecasting the potential domestic and international spread of the 2019-ncov outbreak originating in wuhan, china: a modelling study. *The Lancet*, 395(10225):689–697, 2020.
- [3] Xingjie Hao, Shanshan Cheng, Degang Wu, Tangchun Wu, Xihong Lin, and Chaolong Wang. Reconstruction of the full transmission dynamics of covid-19 in wuhan. *Nature*, 584(7821):420–424, 2020.
- [4] Tao Zhou, Quanhui Liu, Zimo Yang, Jingyi Liao, Kexin Yang, Wei Bai, Xin Lu, and Wei Zhang. Preliminary prediction of the basic reproduction number of the wuhan novel coronavirus 2019-ncov. *Journal of Evidence-Based Medicine*, 13(1):3–7, 2020.
- [5] Zhidong Cao, Qingpeng Zhang, Xin Lu, Dirk Pfeiffer, Lei Wang, Hongbing Song, Tao Pei, Zhongwei Jia, and Daniel Dajun Zeng. Incorporating human movement data to improve epidemiological estimates for 2019-ncov. *medRxiv*, 2020.
- [6] Chernet Tuge Deressa and Gemechis File Duressa. Modeling and optimal control analysis of transmission dynamics of covid-19: The case of ethiopia. *Alexandria Engineering Journal*, 2020.
- [7] Wei-jie Guan, Zheng-yi Ni, Yu Hu, Wen-hua Liang, Chun-quan Ou, Jian-xing He, Lei Liu, Hong Shan, Chun-liang Lei, David SC Hui, et al. Clinical characteristics of 2019 novel coronavirus infection in china. *MedRxiv*, 2020.
- [8] Sheikh Taslim Ali, Lin Wang, Eric HY Lau, Xiao-Ke Xu, Zhanwei Du, Ye Wu, Gabriel M Leung, and Benjamin J Cowling. Serial interval of sars-cov-2 was shortened over time by nonpharmaceutical interventions. *Science*, 369(6507):1106–1109, 2020.
- [9] Kieran A Walsh, Susan Spillane, Laura Comber, Karen Cardwell, Patricia Harrington, Jeff Connell, Conor Teljeur, Natasha Broderick, Cillian F de Gascun, Susan M Smith, et al. The duration of infectiousness of individuals infected with sars-cov-2. *Journal of Infection*, 2020.
- [10] Daihai He, Shi Zhao, Xiaoke Xu, Qiangying Lin, Zian Zhuang, Pei-Hua Cao, Maggie Wang, Yijun Lou, Li Xiao, Ye Wu, and Lin Yang. Low dispersion in the infectiousness of covid-19 cases implies difficulty in control. *BMC Public Health*, 10 2020.
- [11] Salah Ghamizi, Renaud Rwemalika, Maxime Cordy, Lisa Veiber, Tegawendé F Bissyandé, Mike Papadakis, Jacques Klein, and Yves Le Traon. Data-driven simulation and optimization for covid-19 exit strategies. In *Proceedings of the 26th ACM SIGKDD International Conference on Knowledge Discovery & Data Mining*, pages 3434–3442, 2020.
- [12] Jinchang Ren, Yijun Yan, Huimin Zhao, Ping Ma, Jaime Zabalza, Zain Hussain, Shaoming Luo, Qingyun Dai, Sophia Zhao, Aziz Sheikh, et al. Derivation and validation of a novel intelligent computational approach to model epidemiological trends and assess the impact of non-pharmacological interventions for covid-19. *IEEE journal of biomedical and health informatics*, 2020.
- [13] Domenico Gaglione, Paolo Braca, Leonardo Maria Millefiori, Giovanni Soldi, Nicola Forti, Stefano Marano, Peter K Willett, and Krishna R Pattipati. Adaptive bayesian learning and forecasting of epidemic evolution—data analysis of the covid-19 outbreak. *IEEE Access*, 8:175244–175264, 2020.
- [14] William Marciel de Souza, Lewis Fletcher Buss, Darlan da Silva Candido, Jean Paul Carrera, Sabrina Li, Alexander Zarebski, Maria Vincenti-Gonzalez, Janey Messina, Flavia Cristina da Silva Sales, Pamela dos Santos Andrade, et al. Epidemiological and clinical characteristics of the early phase of the covid-19 epidemic in brazil. *medRxiv*, 2020.
- [15] Qianyue Hao, Lin Chen, Fengli Xu, and Yong Li. Understanding the urban pandemic spreading of covid-19 with real world mobility data. In *KDD '20: The 26th ACM SIGKDD Conference on Knowledge Discovery and Data Mining*, 2020.

- [16] Jayson S Jia, Xin Lu, Yun Yuan, Ge Xu, Jianmin Jia, and Nicholas A Christakis. Population flow drives spatio-temporal distribution of covid-19 in china. *Nature*, pages 1–5, 2020.
- [17] Jizhou Huang, Haifeng Wang, Miao Fan, An Zhuo, Yibo Sun, and Ying Li. Understanding the impact of the covid-19 pandemic on transportation-related behaviors with human mobility data. In *Proceedings of the 26th ACM SIGKDD International Conference on Knowledge Discovery & Data Mining*, pages 3443–3450, 2020.
- [18] Xian-Xian Liu and Simon Fong. Towards a realistic model for simulating spread of infectious covid-19 disease. In *Proceedings of the 2020 the 4th International Conference on Big Data and Internet of Things*, pages 96–101, 2020.
- [19] Degang Xu, Xiyang Xu, and Zhifang Su. Novel sivr epidemic spreading model with virus variation in complex networks. In *The 27th Chinese Control and Decision Conference (2015 CCDC)*, pages 5164–5169. IEEE, 2015.
- [20] I Nino, M Fernandez, M De la Sen, S Alonso-Quesada, R Nistal, and Asier Ibeas. About two compared seiadr and seir discrete epidemic models. In *2019 17th International Conference on ICT and Knowledge Engineering (ICT&KE)*, pages 1–6. IEEE, 2019.
- [21] Qian Zhang, Nicola Perra, Daniela Perrotta, Michele Tizzoni, Daniela Paolotti, and Alessandro Vesagnani. Forecasting seasonal influenza fusing digital indicators and a mechanistic disease model. In *Proceedings of the 26th international conference on world wide web*, pages 311–319, 2017.
- [22] Hemant Bherwani, Ankit Gupta, Saima Anjum, Avneesh Anshul, and Rakesh Kumar. Exploring dependence of covid-19 on environmental factors and spread prediction in india. *npj Climate and Atmospheric Science*, 3(1):38, Sep 2020.
- [23] Wandong Zhang, WG Will Zhao, Dana Wu, and Yimin Yang. Predicting covid-19 trends in canada: a tale of four models. *Cognitive Computation and Systems*, 2(3):112–118, 2020.
- [24] Massimo A Achterberg, Bastian Prasse, Long Ma, Stojan Trajanovski, Maksim Kitsak, and Piet Van Mieghem. Comparing the accuracy of several network-based covid-19 prediction algorithms. *International Journal of Forecasting*, 2020.
- [25] Huaiyu Tian, Yonghong Liu, Yidan Li, Chieh-Hsi Wu, Bin Chen, Moritz UG Kraemer, Bingying Li, Jun Cai, Bo Xu, Qiqi Yang, et al. An investigation of transmission control measures during the first 50 days of the covid-19 epidemic in china. *Science*, 368(6491):638–642, 2020.
- [26] Zhanwei Du, Xiaoke Xu, Lin Wang, Spencer J Fox, Benjamin J Cowling, Alison P Galvani, and Lauren Ancel Meyers. Effects of proactive social distancing on covid-19 outbreaks in 58 cities, china. *Emerging infectious diseases*, 26(9):2267, 2020.
- [27] Canelle Poirier, Wei Luo, Maimuna S Majumder, Dianbo Liu, Kenneth Mandl, Todd Mooring, and Mauricio Santillana. The role of environmental factors on transmission rates of the covid-19 outbreak: An initial assessment in two spatial scales. *Available at SSRN 3552677*, 2020.
- [28] Zhen Jin. *Mathematical Modeling and Research on Dynamics of Infectious Diseases*. 2004.